Effect of the excitation pulse carrier frequency on the ultrafast charge recombination dynamics of donor-acceptor complexes: Stochastic simulations and experiments

Roman G. Fedunov, Serguei V. Feskov, and Anatoly I. Ivanov[a)]
Department of Physics, Volgograd State University, 2-nd Prodolnaya Str., 30, Volgograd, 400062, Russia

Olivier Nicolet, Stéphane Pagès, and Eric Vauthey[b)]
Department of Physical Chemistry, University of Geneva, 30 Quai Ernest Ansermet, CH-1211 Geneva 4, Switzerland

(Received 12 April 2004; accepted 20 May 2004)

The influence of the excitation pulse carrier frequency on the ultrafast charge recombination dynamics of excited donor-acceptor complexes has been explored both theoretically and experimentally. The theoretical description involves the explicit treatment of both the optical formation of the nuclear wave packet on the excited free energy surface and its ensuing dynamics. The wave packet motion and the electronic transition are described within the framework of the stochastic point-transition approach. It is shown that the variation of the pulse carrier frequency within the absorption band can significantly change the effective charge recombination dynamics. The mechanism of this phenomenon is analyzed and a semiquantitative interpretation is suggested. The role of the vibrational coherence in the recombination dynamics is discussed. An experimental investigation of the ultrafast charge recombination dynamics of two donor-acceptor complexes in valeronitrile also is presented. The decays of the excited state population were found to be highly nonexponential, the degree of non-exponentiality depending on the excitation frequency. For one complex, the charge recombination dynamics was found to slow down upon increasing the excitation frequency, while the opposite behavior was observed with the other complex. These experimental observations follow qualitatively the predictions of the simulations. © *2004 American Institute of Physics.* [DOI: 10.1063/1.1772362]

I. INTRODUCTION

The optical excitation of a molecule by a short pump pulse results in the population of a nonequilibrium vibrational state on the upper free energy surface. If the excited electronic state population decays within a time scale shorter or comparable to that of nuclear relaxation, this nonequilibrium vibrational population can be expected to affect the decay dynamics. The vibrational nonequilibrium is most conspicuous in vibrational coherence. Early direct observations of the occurrence of vibrational coherence in the dynamics of elementary chemical reactions were related to the bond breakage of diatomic molecules in the gas phase.[1] In those experiments, the passage of the vibrational wave packet through the curve crossing point was visualized as a stepwise increase of the product state population. Coherent vibrational motion on excited state surfaces has also been observed in charge transfer processes in the condensed phase.[2–4]

Pump-probe measurements have demonstrated the widespread occurrence of vibrational coherence in molecular systems excited by an ultrashort laser pulse. The influence of nonequilibrium and especially coherent vibrational motion on electronic transitions has received considerable attention in theoretical studies of both time-dependent fluorescence[5–11] and electron transfer (ET) reactions.[12–20] The coherent underdamped motion on the reactant free energy surface results in a variety of subtle effects on the reaction dynamics.[17,18,21,22] In this case, every visit of the wave packet in the term crossing region (TCR) has to lead to a stepwise decrease of the reactant state population. Reverse transitions from the nonrelaxed product state are also possible and make the ET dynamics more complex. However, the direct observation of the influence of the coherence of the reactant state on the ET dynamics still remains a challenging task.[23] The discussions of the effect of coherence on the ET dynamics have essentially concentrated on systems with underdamped vibrational motion. In this paper, the influence of coherent vibrational motion on the effective ET rate in systems with overdamped nuclear motion is explored.

To avoid any confusion, it has to be pointed out that the term vibrational coherence is used here to design any vibrational state with the wave packet center of gravity located away from the minimum of the excited free energy surface. In a photoinduced ET, the initial nuclear state of the system is in nonequilibrium and thus depends on the characteristics of the excitation pulse. Therefore, the ultrafast ET dynamics should depend on both the physical properties of the ET system and the spectral characteristics of the excitation pulse. As a consequence, a proper theoretical description of ultrafast ET requires the explicit treatment of both the optical formation of the nuclear wave packet on the excited free

[a)]Electronic mail: physic@vlink.ru
[b)]Electronic mail: eric.vauthey@chiphy.unige.ch

energy surface and its ensuing dynamics. The calculations of the ET dynamics are performed within the framework of the stochastic point-transition approach that was originally suggested in Refs. 24 and 25 and later extended in different aspects.[26–29] This approach has been firmly established in the so-called spin-boson model of ET.[30–32]

The aim of this paper is to investigate the influence of the spectral characteristics of the pump pulse on the ultrafast charge recombination (CR) dynamics of donor-acceptor complexes (DAC). To evaluate this spectral effect, numerical simulations of the multi-dimensional diffusion dynamics are applied. Experimental measurements of the ultrafast CR dynamics of several DACs in polar solvents upon excitation at different wavelengths are presented and the results are compared the predictions of the theoretical model. The remainder of this paper is organized as follows: Section II outlines the basic concepts of the model; Sec. III discusses the results of CR dynamics simulations and mechanisms of the spectral effect; the experimental measurements are described and discussed in Sec. IV, and concluding remarks are presented in Sec. V.

II. MODEL

DACs in solution are particularly well suited to study the spectral effects. These complexes are characterized by a broad charge-transfer absorption band that allows the carrier frequency of the pump pulse to be varied over a sufficiently wide range. The excited state associated with this transition is essentially a contact ion pair, that can either dissociate into free ions or decay radiatively or nonradiatively back to the ground state. In many DACs, the latter process, which corresponds to a CR is ultrafast and is thus the major deactivation pathway of the contact ion pair.[33–46]

In the following, we will only consider the nonadiabatic reaction, and assume that the electronic transitions are only possible if the energies of the excited and ground states of the complex are equal, in accordance to the Franck-Condon principle. We will refer to these nuclear configurations as the TCR.

Generally, one can distinguish two pathways for the system to reach the TCR. If the nuclear subsystem is initially in the statistical equilibrium, the TCR is likely to be populated through thermal activation. This is the case of the thermal ET, which has been the focus of attention in many studies in solution. A different situation appears when the initial nuclear state is out of equilibrium. In this case, the TCR can be reached *in the course* of nuclear relaxation. In the latter case, the ET dynamics seem to be even more sensitive to the details of relaxation dynamics than in the thermal case. This leads to several phenomena, which are investigated in this paper.

We consider CR in DACs as a two term crossing problem. The model includes the ground $|g\rangle$ and the first excited $|e\rangle$ electronic states of the complex, which are coupled both radiatively by a nonzero transition dipole moment $\vec{d}$, and nonradiatively by an electron exchange matrix element V_{el}. Higher electronic excited states are assumed not to be involved in ET. This imposes obvious restrictions on both the absorption spectrum of the DAC and the spectral characteristics of the pump pulse.

Just before an optical excitation, the electronic subsystem is assumed to be in the ground state and the nuclear subsystem to be in thermal equilibrium. The latter can thus be described by a Boltzmann distribution in the phase space. A short laser pulse produces a wave packet on the excited free energy surface. The shape of this initial wave packet is determined by the characteristics of the pump pulse. The prepared wave packet tends to occupy an equilibrium position, giving rise to the relaxation of the nuclear modes coupled to ET. During relaxation, the wave packet is likely to reach the reactive zone where CR can take place.

The electronic transitions considered interact strongly with both high-frequency intramolecular vibrations of the complex, and nuclear degrees of freedom of the solvent. The optical pulses used in experiments have a typical duration of 50–100 fs and a rather narrow spectrum. After excitation, the high-frequency degrees of freedom appear therefore either in one of the stationary states or in an incoherent mixture of stationary states. The relaxation time of high-frequency vibrations in large organic molecules, like the constituants of DACs, τ_{rv}, is known to be of the order of 50 fs.[47] For a CR process with characteristic time scales larger than τ_{rv}, the influence of the intramolecular vibrations on the magnitude of the spectral effect should thus not be significant. This is supported by the results obtained within the framework of nonstationary perturbation theory.[20] For this reason, and also to clear up the mechanism of the spectral effect caused by the solvent, a model which does not include intramolecular high-frequency vibrations is investigated in this paper. Nevertheless, the quantitative description of the spectral effect may require these vibrations to be accounted for and such a research is planned in the near future.

An essential element of ET theories is the concept of reaction coordinate as a quantity describing the collective behavior of nuclear degrees of freedom of the system during the elementary act of the reaction. As a reaction coordinate, it is convenient to choose the energy difference ΔE of the two electronic states participating to the process, at a given position of the nuclei.[24] Obviously, ET becomes only possible when $\Delta E=0$ and the chemical transformation is associated with the single degree of freedom $\Delta E(t)$ only. The remaining degrees of freedom form a bath and manifests themselves in the dynamic properties of the reaction coordinate.

The main dynamic characteristic of the reaction coordinate is its autocorrelation function $K(t)=\langle \Delta E(t)\Delta E(0)\rangle$, where the angular brackets denote the averaging over the bath states. For ET reactions in polar solvents, the interaction between the transferred charge and the solvent polarization fluctuations plays the dominant role, and the autocorrelation function is expressed in terms of the complex dielectric susceptibility of the solvent.[24,48] The Debye model of polar solvents was shown to correspond to a Markovian random process $\Delta E(t)$ with an autocorrelation function[24]

$$K(t)=K(0)\exp(-t/\tau_L),$$

where τ_L is the longitudinal dielectric relaxation time of the solvent, $K(0)=2E_r k_B T$ is the thermal dispersion of the re-

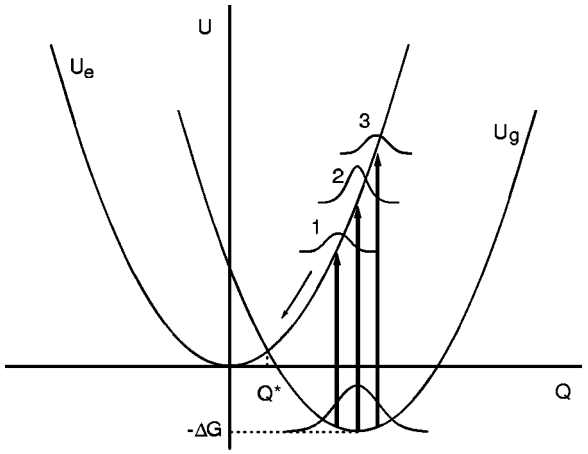

FIG. 1. Diabatic free energy curves of the ground U_g and excited U_e electronic states. The optical excitation of the system is represented by the arrows, whose lengths are proportional to the excitation frequency. The numbers 1,2,3 are the initial positions of the wave packet in the excited state.

action coordinate, E_r is the reorganization energy of the nuclear degrees of freedom, k_B is the Boltzmann constant, and T is the temperature.

In real systems, more complex $K(t)$ functions that can be frequently described by several relaxation times τ_i have been reported.[49] In this case, the autocorrelation function can be satisfactory approximated by a sum of several exponential

$$K(t)=\sum_i K_i(t), \quad K_i(t)=K(0)\,\delta_i \exp(-t/\tau_i),$$

where $\Sigma_i \delta_i = 1$. It allows the generalized coordinate $\Delta E(t)$ to be expressed as a sum of statistically independent variables $E_i(t)$, each of them being Markovian and characterized by an exponential autocorrelation function with the relaxation time τ_i and the dispersion $K_i(0)=2E_r k_B T \delta_i = 2E_{ri} k_B T$. The evolution of $E_i(t)$ can be considered as a motion along an appropriate coordinate Q_i, which is further referred to as a nuclear mode, or a reaction coordinate. Then, the quantity $E_{ri}=E_r \delta_i$ represents the reorganization energy of ith mode.

Hereafter, we will consider both exponential and biexponential autocorrelation functions. It has been pointed out that this approximation gives a satisfactory description of the fluctuation dynamics in many real solvents.[50,51]

The free energy surfaces of the ground U_g and excited electronic state U_e of a DAC can be expressed in terms of the reaction coordinates Q_1 and Q_2[52]

$$U_e=\sum_i \frac{Q_i^2}{4E_{ri}}, \quad U_g=\sum_i \frac{(Q_i-2E_{ri})^2}{4E_{ri}}+\Delta G, \tag{1}$$

where ΔG is the free energy of the CR reaction. By definition, Q_1 will be assumed to be the fast mode with the relaxation time τ_1, and Q_2 to be the slow one with the time constant τ_2. Sections of the free energy surfaces along one of these coordinates are illustrated in Fig. 1.

A set of diffusion equations for the probability distributions $\rho_{ij}(\vec{Q},t)$ can now be written[24,25]

$$\frac{\partial \varrho_{ee}(\vec{Q},t)}{\partial t}=\hat{L}_e \varrho_{ee}(\vec{Q},t)-k(\vec{Q})[\varrho_{ee}(\vec{Q},t)-\varrho_{gg}(\vec{Q},t)], \tag{2}$$

$$\frac{\partial \varrho_{gg}(\vec{Q},t)}{\partial t}=\hat{L}_g \varrho_{gg}(\vec{Q},t)-k(\vec{Q})[\varrho_{gg}(\vec{Q},t)-\varrho_{ee}(\vec{Q},t)], \tag{3}$$

where

$$\hat{L}_e=\sum_i \frac{1}{\tau_i}\left(1+Q_i\frac{\partial}{\partial Q_i}+\langle Q_i^2\rangle \frac{\partial^2}{\partial Q_i^2}\right),$$

$$\hat{L}_g=\sum_i \frac{1}{\tau_i}\left(1+(Q_i-2E_{ri})\frac{\partial}{\partial Q_i}+\langle Q_i^2\rangle \frac{\partial^2}{\partial Q_i^2}\right),$$

with $\langle Q_i^2\rangle = 2E_{ri}k_B T$ is the dispersion of the thermal distribution along the ith coordinate,

$$k(\vec{Q})=k_0\,\delta(U_e-U_g)=\frac{2\pi V_{\mathrm{el}}^2}{\hbar}\,\delta(z-z^{\#}), \tag{4}$$

with $z=Q_1+Q_2$, $z^{\#}=E_r+\Delta G$.

This set of equations should be completed with the initial conditions for $\varrho_{ee}(\vec{Q},0)$ and $\varrho_{gg}(\vec{Q},0)$. The initial distribution, $\varrho_{ee}(\vec{Q},0)$, is calculated in Appendix B. It depends explicitly on the spectral characteristics of the laser pulse and is given by Eq. (B18). The ground state is assumed to be empty, i.e., $\varrho_{gg}(\vec{Q},0)=0$.

III. NUMERICAL RESULTS AND DISCUSSION

Before discussing the results of the numerical calculations, we briefly explain the choice of the model parameters. For ET reactions in strongly polar solvents (acetonitrile, alcohols, and others), the solvent reorganization energy is usually of the order of $E_r=1$ eV,[45,53] and this value will thus be used further on. These solvents are characterized by two, three, or even more relaxation times. The shorter relaxation time constant is of the order of 0.2–1 ps, and the longer one of the order of 5–10 ps.[54–56] The simulations have thus been carried out with such time constants.

The range of CR free energy ΔG, with known DACs varies from about -3 eV up to less than -1 eV,[33,34,46] and this whole spectrum will thus be considered. The magnitude of the electronic matrix element can vary over a wide range. There is however no consistent information on its value. Although DACs with V_{el} close to 1 eV most certainly exist, the model used here is only applicable for nonadiabatic reactions with a rather small V_{el}, i.e., $V_{\mathrm{el}}<k_B T$.[57] Therefore, the investigation of the spectral effect is limited to this range of V_{el}. For substantially larger V_{el}, the adiabatic theory of electronic transitions has to be applied.[58,59]

The formulation of the model assumes that the duration of the pump pulse is significantly smaller than the relaxation time scale of the solvent. Therefore, the wave packet motion on the excited state surface and the CR during the pumping stage can be neglected. To satisfy this restriction, a pulse duration of $\tau_e=50$ fs was chosen. Typical time profiles of the excited state population are shown in Fig. 2. They indi-

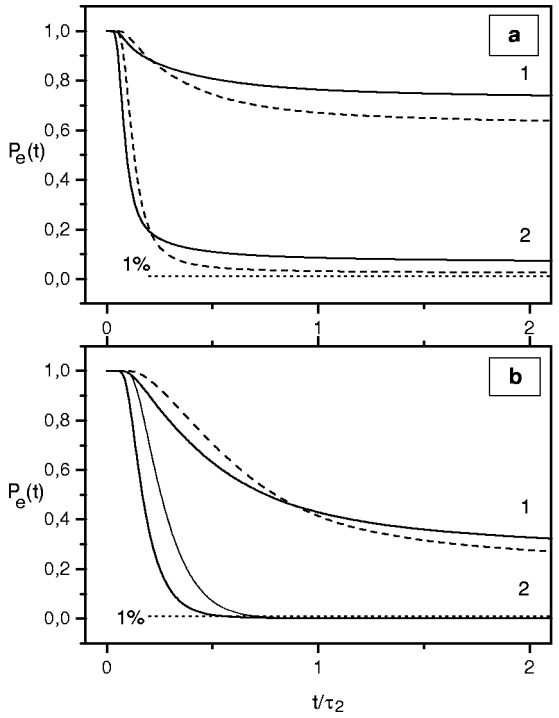

FIG. 2. Excited state population dynamics due nonthermal ET reaction for a model including two Debye-like modes. The parameters used here are $T=300$ K, $\tau_e=50$ fs, $\tau_1=500$ fs, $\tau_2=10$ ps, $E_{r1}=0.7$, $E_{r2}=0.3$, (1) $V_{\mathrm{el}}=0.0050$; (2) $V_{\mathrm{el}}=0.0245$; (a) $\Delta G=-0.3$; (b) $\Delta G=-0.7$. Dashed lines: high frequency excitation; solid lines: low-frequency excitation. All energies are in electron volts.

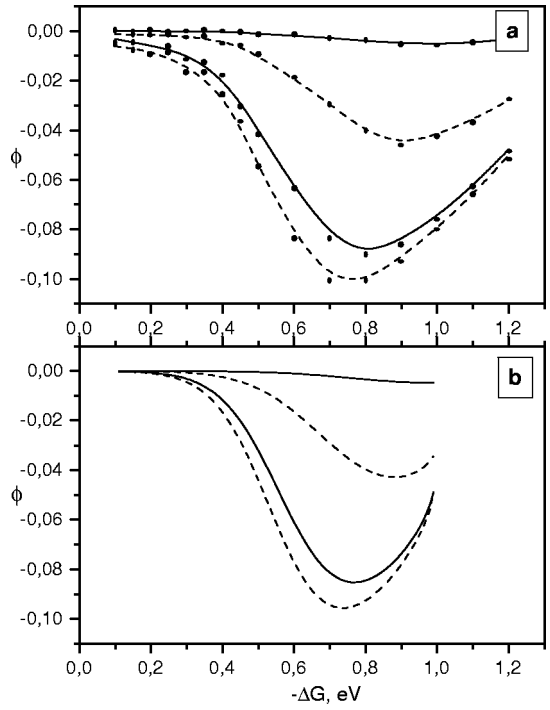

FIG. 3. Free energy dependence of the spectral effect ϕ for a single Debye mode model. (a) Stochastic simulation, the dots are the results of the numerical simulations; (b) results obtained from the average trajectory approach. The parameters used here are $T=300$ K, $\tau_e=50$ fs, $E_r=1$ eV, $\tau_1=500$ fs (solid lines) and $\tau_1=10$ ps (dashed lines); (1), (2) $V_{\mathrm{el}}=0.015$ eV; (3), (4) $V_{\mathrm{el}}=0.0245$ eV.

cate that the electronic transitions in the system start within a time scale similar to that of relaxation. It should also be noted that for the parameters chosen, a twofold change of τ_e has no significant influence on the magnitude of the spectral effect.

In this section, the results of a series of numerical simulations with a single mode and a two mode model are presented. The Brownian simulation algorithm (Appendix A) has been used to calculate the time-dependent populations of the electronic states. The simulation program was run on a Pentium IV 2GHz PC and each simulation in the interval $[0,10\tau_2]$ required about eight hours. A satisfactory convergence of the results was achieved with 10^5-10^6 trajectories.

The simulations presented in Fig. 2 show that excited state population dynamics is nonexponential and depends substantially on the pump pulse frequency. For a quantitative estimation of the influence of the excitation pulse frequency on the CR dynamics, we introduce a time-independent effective rate constant

$$k_{\mathrm{eff}}^{-1}=\int_0^{t_0}P_e(t_1)dt_1, \tag{5}$$

where $P_e(t)$ is the population of the charge separated state, $[0,t_0]$ is the time interval after which $P_e(t)$ reduces down to 0.01 of its initial value, as it is typically monitored in an experiment.

The spectral effect is defined as

$$\phi=\frac{k_{\mathrm{eff}}(\omega_e^+)-k_{\mathrm{eff}}(\omega_e^-)}{k_{\mathrm{eff}}(\omega_e^-)}, \tag{6}$$

where $k_{\mathrm{eff}}(\omega_e^+)$ and $k_{\mathrm{eff}}(\omega_e^-)$ are the effective rate constants after excitation at the frequencies ω_e^+ and ω_e^- defined as

$$\omega_e^{\pm}=E_r-\Delta G\pm 2\sqrt{E_r k_B T\ln 2}$$

and corresponding to the frequencies at the half-maximum of the charge transfer absorption band. Therefore, a positive spectral effect implies that the CR after *high* frequency excitation proceeds *faster* than upon low frequency excitation.

A. Single Debye mode model

The calculations of the spectral effect were first carried out with a model including a single Debye mode Q with a characteristic relaxation time τ_1. This model reproduces the original Zusman's formulation of ET in polar solvents, Q corresponding to the solvent collective polarization mode, and τ_1 being the longitudinal relaxation time.[24]

The simulations reveal a negative spectral effect over the whole range of the parameters ΔG, V_{el}, and τ_1, covering low- and high-barrier processes from the deep nonadiabatic to the solvent-controlled regime. Figure 3(a) shows the dependence of ϕ on the reaction free energy ΔG for some values of the electronic coupling V_{el} and of the relaxation time τ_1. The spectral effect has been found to have a strong dependence on the Zusman parameter, g, as it can be expected from an analysis of the dimensionality of Eqs. (2,3)

$$g=\frac{2\pi V_{\mathrm{el}}^2\tau_L}{\hbar E_r}. \tag{7}$$

It should be emphasized that a variation of the parameters V_{el}, τ_L, and E_r, provided that g is kept constant, does not change the spectral effect.

The spectral effect ϕ is negative over the whole free energy range and is the strongest, $\phi=\phi_{\max}$, around $-\Delta G=E_r$, where the processes is barrierless. The absolute value of $\phi_{\max}$ increases with g and saturates in the strong solvent-controlled regime.

The results pictured in Fig. 3(a) have a rather transparent physical interpretation. As illustrated in Fig. 1, the initial position of the wave packet immediately after excitation at the frequency ω_e^+ is far from the term crossing point and some additional time Δt is thus required to reach the reactive zone. Denoting $k_{\mathrm{eff}}^{-1}(\omega_e^-)=t_0$, one can write $k_{\mathrm{eff}}^{-1}(\omega_e^+)=t_0+\Delta t$, and hence $\phi=-\Delta t/(\Delta t+t_0)$. The time delay Δt is essentially independent of the driving force. However, in the normal region $-\Delta G<E_r$, the effective reaction time t_0 decreases with increasing driving force and therefore the spectral effect becomes stronger.

According to the Marcus activation factor, the thermal CR rate and t_0^{-1} should reach their maximum value for activationless reaction, and therefore the strongest spectral effect is expected to occur in the vicinity of $-\Delta G=E_r$. However, this simple picture can only be justified if the thermal transitions play a determinant role.

As it can be seen in Fig. 3(a), the increase of both τ_1 and V_{el} results in a shift of $\phi_{\max}$ to smaller driving forces. This implies that t_0 has its minimum around $-\Delta G<E_r$. This can be understood if one takes into account that, in this case, the nonthermal transitions play a significant role and their time scale t_0 increases with the driving force.

B. Two Debye modes model

The presence of two distinct time scales of nuclear relaxation makes the picture of the CR dynamics somewhat different. In this case the initial position of the wave packet becomes more important. As illustrated in Fig. 4, the wave packets prepared by ω^+ and ω^- pulses follow quite *different paths* to the equilibrium position. Obviously, these paths cross the reactive region in distinct areas of the phase space. In this case, considerable changes of the CR effective rate constant should expected when the details of the preparation of the initial state are altered.

The free energy dependence of the spectral effect is pictured in Fig. 5(a). Surprisingly, a positive spectral effect can be seen in the low exergonicity region. With the parameters used here, this positive spectral effect takes place between $-\Delta G=0.1$ eV and $-\Delta G=0.6$ eV. The positive spectral effect can be interpreted in terms of rather simple concepts characterizing the wave packet motion on the free energy surface.

With the parameters used here ($V_{\mathrm{el}}=k_BT$), the positive spectral effect peaks at $-\Delta G=0.3$ eV, and the negative spectral effect has its maximum around $-\Delta G=0.6$ eV. A decrease of V_{el} results in a decrease of the magnitude of both the positive and negative spectral effects.

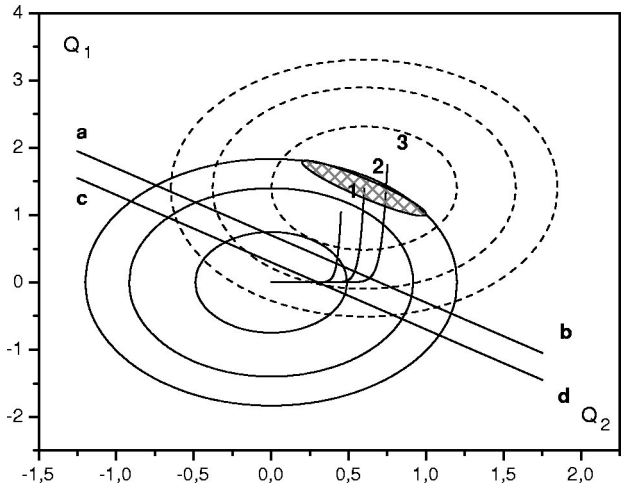

FIG. 4. Wave packet trajectories on the excited free energy surface for a two Debye modes model. The dashed and solid lines are the equipotential curves of the ground and excited states, respectively. The dark ellipse is the wave packet created by an excitation pulse with $\tau_e=50$ fs. The term crossing lines are labeled ab for $\Delta G=-0.3$ and cd for $\Delta G=-0.7$. The parameters used here are: $\tau_1=500$ fs, $\tau_2=10$ ps, $E_{r1}=0.7$, $E_{r2}=0.3$. All energies are in electron volts.

One can expect that the positive spectral effect culminates when the term crossing line passes through the wave-packet trajectory number 2 at its sharp bend (see Fig. 4). Indeed, in this case blue and red wave packets intersect the term crossing line while moving along the slow and the fast coordinate, respectively.

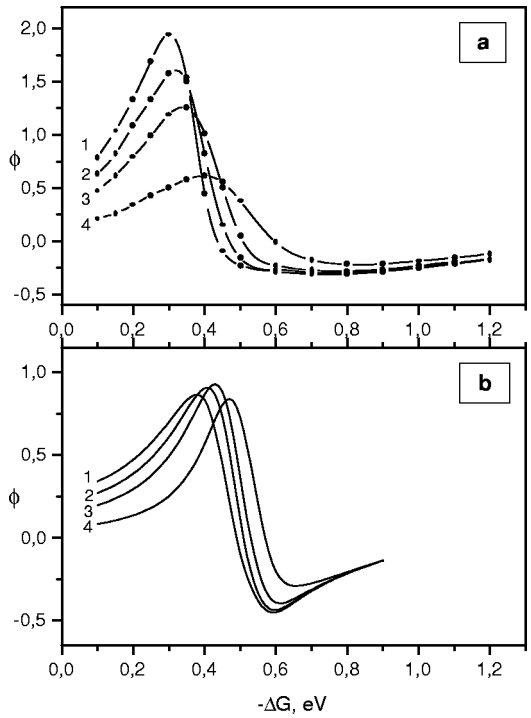

FIG. 5. Free energy dependence of the spectral effect ϕ for the two Debye modes model. (a) Stochastic simulations, the dots are the results of the numerical simulations; (b) results obtained from the average trajectory approach. The parameters used here are: $T=300$ K, $\tau_e=50$ fs, $\tau_1=500$ fs, $\tau_2=10$ ps, $E_{r1}=0.7$, $E_{r2}=0.3$; (1) $V_{\mathrm{el}}=0.0245$; (2) $V_{\mathrm{el}}=0.0150$; (3) $V_{\mathrm{el}}=0.0100$; (4) $V_{\mathrm{el}}=0.0050$. All energies are in electron volts.

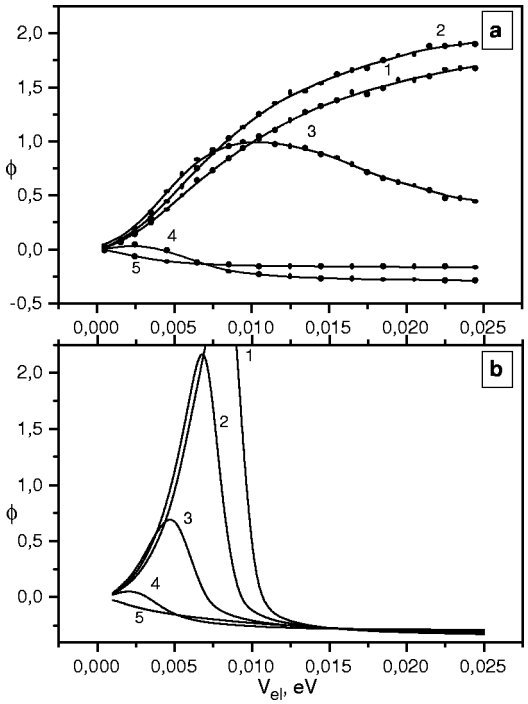

FIG. 6. Dependence of the spectral effect ϕ on the electronic coupling V_{el}. (a) The dots are the results of stochastic simulations; (b) results from the time-dependent golden rule (Ref. 20). (b) The parameters used here are: $T=300$ K, $\tau_e=50$ fs, $\tau_1=500$ fs, $\tau_2=10$ ps, $E_{r1}=0.7$, $E_{r2}=0.3$, (1) $\Delta G=-0.25$; (2) $\Delta G=-0.3$; (3) $\Delta G=-0.4$; (4) $\Delta G=-0.6$; (5) $\Delta G=-1.2$. All energies are in electron volts.

This condition implies that the maximum positive spectral effect should be around $-\Delta G=E_{r1}-E_{r2}$. The calculations confirm that the maximum lies in the vicinity of this point, although there is a weak dependence on the electron coupling V_{el}. It should be stressed that the positive spectral effect can only be expected if the inequality $E_{r1}-E_{r2}>0$ is satisfied.

The dependence of the spectral effect on the electronic coupling V_{el} is shown in Fig. 6(a). The weak scattering of the points is due to the systematic inaccuracy caused by the stochastic simulation for $N=2.5\times10^5$ trajectories, which should become negligible when $N>10^6$. Curves 1 and 2 depict the monotonic increase of the positive spectral effect with the electronic coupling. Such behavior is typical for the low exergonicity region. It should be noted that, since the solvent controlled limit has already been reached, a further increase of V_{el} results in a weak change of ϕ.

A different behavior is observed when $-\Delta G>E_{r1}-E_{r2}$. In this case, the dependence of the spectral effect on V_{el} is nonmonotonous because of the increasing role of the thermal electron transfer process. Increasing the driving force results in a considerable decrease of the positive spectral effect. In the Marcus inverted region, $-\Delta G>E_r$, the spectral effect is always negative and changes slowly upon increasing the electronic coupling.

The dependence of the spectral effect on the electronic coupling obtained within the framework of the nonequilibrium Golden Rule for the model with two Debye modes[20] is presented in Fig. 6(b). It can be seen that the Golden Rule results are in good agreement with the stochastic simulations with small electronic coupling. However, Fig. 6(b) shows a considerably different prediction at larger V_{el}.

Numerical simulations of the two-mode model have clearly shown that there is a cardinal difference of spectral effect with the single- and two-mode models. First, both the positive and negative effects are predicted in the latter case. Second, higher absolute values of ϕ should be expected in the two-mode model, reflecting a considerable change of CR dynamics with the variation of the spectral characteristic of the pump pulse.

TABLE I. Parameters obtained from the fit of Eq. (8) to the calculated decays of the excited DAC population. The parameters used are $E_{r1}=0.7$ eV, $E_{r2}=0.3$ eV, $\tau_1=0.5$ ps, $\tau_2=10$ ps, $\eta=\delta\omega_e/2(E_r k_B T \ln 2)^{1/2}$. R is the coefficient of correlation.

η	ΔG(eV)	V_{el}(eV)	τ(ps)	s	R^2
+1	−0.3	0.0025	58.0	0.58	0.960
−1	−0.3	0.0025	78.4	0.64	0.965
+1	−0.6	0.0025	1.81	0.49	0.930
−1	−0.6	0.0025	2.13	0.44	0.959
+1	−0.6	0.0245	0.31	2.45	0.995
−1	−0.6	0.0245	0.21	2.42	0.992
+1	−1.3	0.001	11.3	1.67	0.994
−1	−1.3	0.001	11.0	1.57	0.995
+1	−1.3	0.003	4.66	1.84	0.994
−1	−1.3	0.003	4.29	1.72	0.995
+1	−1.3	0.007	2.82	2.34	0.996
−1	−1.3	0.007	2.54	2.03	0.997

C. Excited state population dynamics

The simulations have shown that the decay of the excited state population is strongly nonexponential for a broad range of parameters. The population dynamics could often be satisfactory reproduced by a function of the following form:

$$f(t)=A\exp(-(t/\tau)^s). \tag{8}$$

Equation (8) reflects a rate dependence on time. If $s>1$ the rate increases with time and it decreases when $s<1$.

The s and τ values obtained from the fit of Eq. (8) to the simulated data are listed in Table I. These results show quantitatively the extent of nonexponentiality of the excited state population dynamics. The following features can be observed:

(1) At weak exergonicity, when the positive spectral effect is predicted, the excited state population dynamics is reproduced by Eq. (8) provided that the electronic coupling is weak. In this case, the parameter s is considerably smaller than unity and its value decreases with increasing excitation frequency.

(2) In the region of larger exergonicity, yet in the Marcus normal region, where negative spectral effect is expected, the parameter s increases with increasing excitation pulse frequency. The s value strongly depends on the electronic coupling, the larger the coupling the larger s. When s is markedly less than unity, the coefficient of correlation is also considerably smaller than unity, that is the fitting is not very good.

(3) In the Marcus inverted region, s is invariably larger than unity. It is a rising function of both the electron coupling and the excitation pulse frequency.

These features can be understood if one considers the motion of the wave packet relatively the term crossing line. In the Marcus normal region, the wave packet invariably intersects the term crossing line during its thermalization. This results in a nonmonotonous time dependence of the rate: In the first stage of thermalization, the rate increases, and then, after the wave packet has passed the term crossing region, the rate decreases. Therefore, Eq. (8) should not be expected to fit the calculated population dynamics very well. If the stage where the rate decreases dominates, i.e., if the probability of CR before the term crossing region is small, the parameter s has to be less than unity. On the other hand, if CR occurs mostly during the first stage of thermalization, i.e., when the rate increases, s will be larger than unity. Both these situations occur in the low exergonicity region.

In the Marcus inverted region, the wave packet does not intersect the term crossing line during thermalization. As a consequence, the rate increases monotonously with time and a s value larger than unity is predicted.

D. Coherence versus incoherence

It should be emphasized that a significant positive spectral effect may only be expected when the vibrational coherence, in the sense mentioned in the Introduction, plays an important role. To show this explicitly, the simulations have been carried out using a nonequilibrium and incoherent wave packet as an initial vibrational state. As an incoherent state, we use a wave packet centered at the excited state minimum but with a much larger width than the thermal wave packet

$$\varrho(\vec{Q},\omega_e,t=0)=\prod_i^M [2\pi\sigma_i^2(\omega_e,0)]^{-1/2} \times \exp\left\{-\frac{Q_i^2}{2\sigma_i^2(\omega_e,0)}\right\}. \quad (9)$$

In order to have the same average vibrational energy of the initial state in both coherent and incoherent cases, the standard deviation is set to $\sigma_i(\omega_e,0)=[4E_{ri}(\Delta G+\omega_e)/M]^{1/2}$, M being the number of Debye-type modes. Indeed, the average energy of the state represented by Eq. (9) is

$$\bar{U}=\int U_e(\vec{Q})\varrho(\vec{Q},\omega_e,t=0)d\vec{Q}=\Delta G+\omega_e,$$

which coincides with the average energy in the state described by Eq. (B18). The evolution of the initial packet Eq. (9) results exclusively in its narrowing.

The free energy dependencies of the spectral effect with such an initial state are pictured in Fig. 7. This figure shows that the positive spectral effect practically vanishes. This is a further confirmation of the crucial role of vibrational coherence in the positive effect. The strongest negative spectral effect is shifted to $-\Delta G=E_r$ and its magnitude remains nearly the same.

Such a dependence of the spectral effect is a direct consequence of the wave packet narrowing during its relaxation.

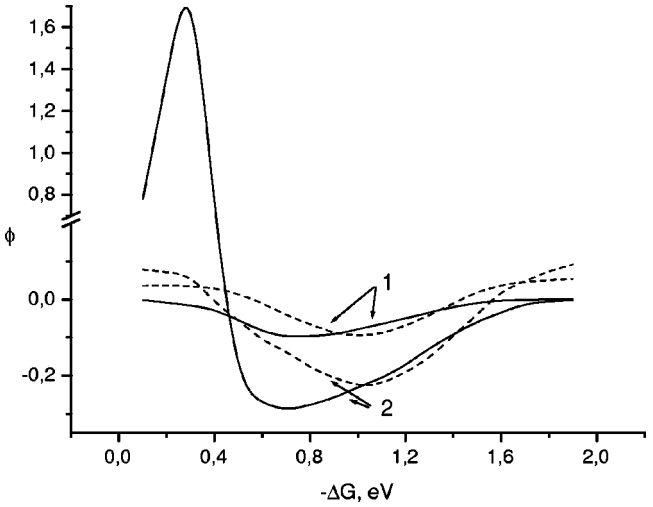

FIG. 7. Free energy dependence of the spectral effect ϕ assuming coherent initial states (solid line) and incoherent initial state (dashed line). The parameters used here are: $T=300$ K, $\tau_e=50$ fs, $V_{el}=0.0245$; (1) $\tau_1=10$ ps, $E_r=1.0$; (2) $\tau_1=500$ fs, $\tau_2=10$ ps, $E_{r1}=0.7$, $E_{r2}=0.3$. All energies are in electron volts.

The decrease of the wave packet width $\sigma_i(\omega_e,t)$ results in an increase of the population near the bottom of the free energy curve. As the CR rate is proportional to the excited state population in the TCR, the rate increases with time if the condition $\langle\Sigma_i\sigma_i^2(\omega_e,t)\rangle^{1/2}>\Delta G+E_r$ is met, the brackets denoting the averaging in the time interval of the reaction t_0. In this case, the rise of the excitation frequency ω_e leads to a decrease of the CR rate, thus to the negative spectral effect. On the other hand, when the term crossing line is far from the excited term minimum, analogous arguments explain the positive spectral effect.

The simulations presented here unambiguously show the importance of the vibrational coherence for the spectral effect.

E. Average trajectory approach

In this subsection, a semiquantitative description of the spectral effect is considered. This approach is only applicable if the nonthermal and the thermal stages of CR are well separated. In this case, the effective rate can be estimated as

$$k_{\text{eff}}^{-1}=t_{\text{nonth}}+t_{\text{therm}}, \quad (10)$$

because the time scale of the reaction is the sum of the time scales of nonthermal and thermal stages.

The time t_{nonth} is associated with the instant where the wave packet maximum passes through the term crossing area. In Fig. 2, this time coincides with the instant where the slope of the population decay is the largest and thus where the rate has its maximum value. This time t_{nonth} depends on the initial position of the wave packet and thus on the carrier frequency of the excitation pulse. The wave packet maximum passes through the term intersection area at time $t^*(\omega_e)$, which can be derived from the equation

$$\sum_i \bar{Q}_i \exp(-t^*/\tau_i)-\Delta G-E_r=0, \quad (11)$$

where $\overline{Q_i}$ is the coordinate of the initial position of the wave-packet maximum determined by Eq. (B19). For an estimation k_{eff} according to Eq. (10), t_{nonth} will, in the following, be taken as $t^*(\omega_e)$.

In the second stage the decay is nearly exponential and its time constant can be approximated by the expression

$$t_{\text{therm}}=[W_e(\omega_e)-\varepsilon]/k_{\text{therm}},$$

where k_{therm} is the thermal CR rate, ε is the fraction of the excited state population at the end of the observation window, W_e is the probability of the wave packet to remain on the excited state surface upon passing the TCR. This quantity is defined as[19]

$$W_e(\omega_e)=1-\frac{2\pi V_{\text{el}}^2}{A_1(\omega_e)}\left(1+2\pi V_{\text{el}}^2\left(\frac{1}{A_1(\omega_e)}+\frac{1}{|A_2(\omega_e)|}\right)\right)^{-1}, \tag{12}$$

$$A_1(\omega_e)=\sum\frac{Q_i^*(\omega_e)}{\tau_i},\quad A_2(\omega_e)=\sum\frac{Q_i^*(\omega_e)-2E_{ri}}{\tau_i},$$

$$Q_i^*(\omega_e)=\overline{Q_i}\exp(-t^*(\omega_e)/\tau_i),$$

where Q_i^* is the value of Q_i at the intersection point. The spectral effect predicted by Eq. (10) is depicted in Figs. 3(b) and 5(b). One can see that the above semiquantitative approach qualitatively reproduces the free energy dependence of the spectral effect. A good agreement is obtained for the one-dimensional model (Fig. 3). For the two-dimensional model, the error on the maximum and minimum of the effect is around 50% (Fig. 5). Moreover, the position of the strongest spectral effect is displaced to the region of higher exergonicity relatively to the numerical calculations.

To understand the mechanism of the spectral effect in the low exergonicity region, let us consider Fig. 2(a). The figure shows that, after terminating the nonthermal stage of the reaction, the excited state population does not reach the value $\varepsilon=0.01$ (the dotted line) even at the greatest possible $V_{\text{el}}=k_BT$. As in the low exergonicity region, the thermal rate is very small, the population P_e decays to ε only after a very long time. Therefore, the contribution of t_{nonth} in Eq. (10) is negligible and the positive spectral effect is defined by the equation

$$\phi=\frac{W_e(\omega_e^+)-W_e(\omega_e^-)}{W_e(\omega_e^-)}.$$

This equation shows that the magnitude of the positive spectral effect is determined by the difference of the probabilities $W_e(\omega_e^+)$ and $W_e(\omega_e^-)$.

It should be emphasized that, in the single mode model, the probabilities $W_e(\omega_e^+)$ and $W_e(\omega_e^-)$ are always identical, and as a result the positive spectral effect vanishes. The reason for the different values of these probabilities in the two-dimensional model becomes clear if one takes into account that the trajectory of the wave packet maximum is determined by both the excitation frequency and the geometry of the electronic terms.

The equipotential lines of the excited and ground electronic states as well as the trajectories of the wave packet maximum are depicted in Fig. 4. The term crossing lines are marked as ab and cd for the low and high exergonicity regimes, respectively. The trajectories number 1, 2, and 3 correspond to small (ω_e^-), medium, and high (ω_e^+) excitation frequency, respectively. The intersection points Q_i^* of the wave packet trajectories with the term crossing line ab, for low and high of ω_e values are at different positions on the free energy surface. The nonthermal transition probability, $1-W_e$ [Eq. (11)], depends on the difference of slope of the tangents of the terms at Q_i^*. If this difference changes upon variation of ω_e, the probabilities $W_e(\omega_e^+)$ and $W_e(\omega_e^-)$ should be expected to be different. It should be stressed that the distance between points $Q_i^*(\omega_e^+)$ and $Q_i^*(\omega_e^-)$ vanishes when $\tau_2\to\tau_1$, and therefore the smaller the difference between the relaxation times, the smaller the magnitude of the positive spectral effect.

In the high exergonicity region [Fig. 2(b)], the contribution of t_{therm} in Eq. (10) is comparable to t^* for trajectory 1 and considerably smaller than t^* for trajectory 2. In the latter case, the spectral effect is negative and can be estimated by the equation

$$\phi=\frac{t^*(\omega_e^+)-t^*(\omega_e^-)}{t^*(\omega_e^-)}.$$

In this case, all the trajectories of the wave packet maximum pass the term crossing line cd at the same point (Fig. 4), and therefore the underlying physics is the same as in the one-dimensional case.

This interpretation not only uncovers the mechanism of the spectral effect but also allows a semiquantitative analysis of this effect.

IV. EXPERIMENTAL RESULTS

Measurements of the occurrence of a spectral effect on the CR dynamics of excited DACs have been performed on complexes composed of pyromellitic dianhydride (PMDA) and tetracyanoethylene (TCNE) as electron acceptors, and substituted benzene derivatives as electron donors in polar solvents. The results obtained with the PMDA complexes have been described briefly in Ref. 60. These complexes were excited at 400 nm and around 530 nm, and the CR dynamics were obtained by monitoring the decay of the $\text{PMDA}^{\cdot-}$ band centerd at 670 nm using the multiplex transient grating (TG) technique.[46] The decay of the excited state population was found to be faster upon 530 nm excitation than upon 400 nm excitation. For example, for the complex 1,2,4-trimethoxybenzene (TMB)/PMDA in valeronitrile (VaCN), the CR time constant was found to increase from 770 ± 80 to 1000 ± 80 fs. This corresponds to a negative spectral effect. There are however two problems associated with these measurements. First, the UV-vis absorption spectrum of the TMB/PMDA complex exhibits two charge transfer (CT) bands. Indeed, upon substitution, the degeneracy of the highest occupied molecular orbitals (HOMOs) of benzene is lifted. Therefore, the two CT bands can be related to two complexes with a distinct geometry.[61,62] While the excitation pulse at 530 nm interacts only with the low frequency band, the 400 nm pulse overlaps with both low and high frequency CT bands. Therefore, the slower CR dynamics ob-

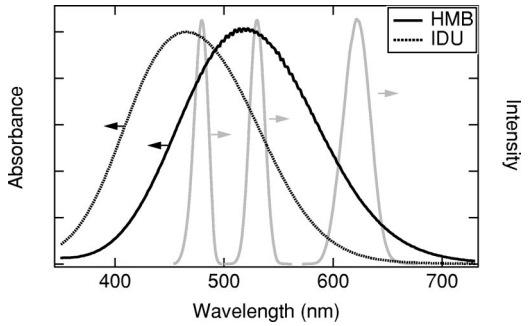

FIG. 8. Absorption spectra of the HMB/TCNE and IDU/TCNE DACs in VaCN and intensity spectra of the laser pulses used for excitation.

served upon 400 nm excitation might also be due to the contribution of DACs with a different geometry rather than to the spectral effect. Second, the multiplex TG technique has been chosen for its high sensitivity.[63] However, this technique is also sensitive to the photoinduced changes of refractive index. Because of this, the TG intensity at very short time is dominated by the optical Kerr effect (OKE) of the solvent, and therefore the determination of the population dynamics during the first few hundreds of femtoseconds is problematic.[45] As shown in Fig. 2, the nonthermal CR results to a strongly nonexponential initial decay of the excited state population. Because of the interference with the OKE, the early excited state dynamics is not easily accessible, and therefore this predicted nonexponentiality could not be verified. In order to avoid these two problems, the excitation frequency dependence of the CR has also been investigated with different DACs and with a different technique. These DACs were composed of TCNE as electron acceptor and several methyl-substituted benzenes as donors in polar solvents. The details of this investigation will be published elsewhere, and therefore only a few representative results are described here.

Figure 8 shows the UV-vis absorption spectra measured with the hexamethylbenzene (HMB)/TCNE and isodurene (1,2,3,5-tetramethylbenzene, IDU)/TCNE complexes in VaCN. Contrarily to the TMB/PMDA complexes, these spectra consist in a single CT band, and thus the first above-mentioned complication is eliminated. This figure also shows the intensity spectra of the excitation pulses. These pulses have been generated with a two-stage noncollinear optical parametric amplifier (NOPA, Clark-MXR Inc., Dexter, Michigan, USA) pumped by a fraction of the output of a 1 kHz Ti:Sapphire amplified system (Spitfire, Spectra-Physics, Mountain View, California, USA). The duration of these pulses after prism recompression was around 45 fs and their energy on the sample was around 250 nJ.

The CR dynamics of these DACs was measured by monitoring the time-evolution of the transmission changes at 400 nm. This wavelength coincides with the absorption spectrum of the radical anion of TCNE.[4,64] The probe pulses were generated upon frequency doubling a fraction of the output pulses of the Ti:Sapphire amplifier. The pulse duration was around 100 fs and the energy on the sample of the order of 20 nJ. The general layout of the transient absorption setup has been described elsewhere.[65] Figure 9 shows the time

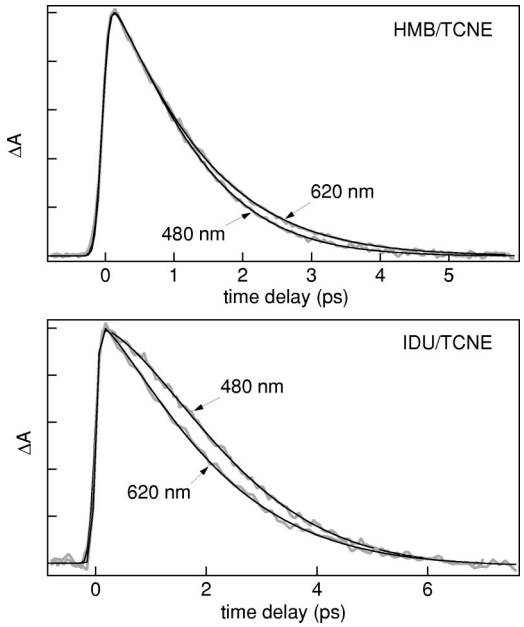

FIG. 9. Time profiles of the transient absorption at 400 nm measured with HMB/TCNE and IDU/TCNE DACs in VaCN after excitation at 480 and 620 nm.

profiles of the transient absorption at 400 nm measured with HMB/TCNE and IDU/TCNE in VaCN after excitation centerd at 620 and 480 nm. The transient absorption at 400 nm increases within the response function of the experimental setup and decays to zero in less than 10 ps. Although, the IDU/TCNE complex exhibits some absorption at 400 nm, its absorption coefficient is too small compared to that of $TCNE^{\cdot -}$ to lead to a significant contribution to the transient signal. On the other hand, the absorbance of the HMB/TCNE complex at 400 nm is negligibly small, and therefore the signal at 400 nm can be safely ascribed to the absorption of $TCNE^{\cdot -}$.

A striking feature of these decays is that none of them is exponential. The continuous lines in Fig. 9 have been obtained by convolving the instrument response function with Eq. (8). This function with $s<1$ is the so-called stretched exponential function.[66] It has been widely used to describe systems exhibiting relaxation in a wide range of time scales. In these cases, the relaxation rate *decreases* with time. However, in order to reproduce the decays shown in Fig. 9, s values larger than unity have to be used, corresponding to a situation where the decay rate *increases* with time. This increase of the decay rate with time is particularly evident with the time profile of IDU/TCNE upon 480 nm excitation. Indeed, once the signal has reached its maximum value, it remains almost constant for about 200 fs before starting to decay. After about 3 ps, the decay is close to exponential. The s and τ values obtained from the fit of Eq. (8) to the decay of HMB/TCNE and IDU/TCNE in VaCN are listed in Table II. The degree of nonexponentiality s is markedly smaller with HMB/TCNE than with IDU/TCNE. However, for both complexes, s increases with increasing excitation frequency. With IDU/TCNE, the lifetime, τ increases with increasing excitation frequency as well. On the other hand, it remains essentially constant with HMB/TCNE. In order to

TABLE II. Parameters obtained from the fit of Eq. (8) to the decays of the excited DAC population and effective time constant, τ_{eff}.

D/A	λ_{exc}(nm)	s	τ(ps)	τ_{eff}(ps)
HMB/TCNE	480	1.31	1.40	1.35
	530	1.26	1.48	1.39
	620	1.19	1.46	1.46
IDU/TCNE	480	1.57	2.75	2.42
	530	1.53	2.70	2.25
	620	1.30	2.30	2.03

compare these results with the predictions of the models described before, an effective decay time constant τ_{eff} as defined in Eq. (5) has also been used. Comparing the data in Table II with the definition of the spectral effect ϕ indicates a positive spectral effect for HMB/TCNE and a negative spectral effect for IDU/TCNE. According to the above theoretical simulations, the magnitude of the spectral effect depends on the time scale of solvent relaxation, on the driving force for CR ΔG and on the magnitude of the electronic coupling V_{el}. In VaCN, the time constant for diffusive solvent relaxation amounts to 4.7 ps.[56] In acetonitrile, where the solvation time is much shorter, around 500 fs,[12] the wavelength dependence of the CR of both HMB/TCNE and IDU/TCNE complexes was found to be hardly detectable, in agreement with the above model. Calculating the driving force for CR as $\Delta G = -E_{\text{ox}}(D) + E_{\text{red}}(A)$, where $E_{\text{ox}}(D)$ and $E_{\text{red}}(A)$ are the oxidation and reduction potential of the donor and acceptor, respectively, results to $\Delta G = -1.35$ and -1.59 eV for HMB/TCNE and IDU/TCNE, respectively. The former value is in agreement with that determined from the analysis of the HMB/TCNE CT absorption band.[67] The occurrence of the negative spectral effect with IDU/TCNE is in agreement with its relatively high exergonicity for CR. On the other hand, the observation of a positive effect with HMB/TCNE is more surprising. According to the above model, the transition from negative to positive spectral effect should occur around $-\Delta G \simeq E_{r1} - E_{r2}$. This means that CR should take place in the normal region. The intramolecular reorganization energy for CR in HMB/TCNE has been found to amount to about 0.45 eV,[67] while the solvent reorganization energy for CR in such complexes has been reported to be around 0.5 eV in polar solvents.[68] According to these values, the total reorganization energy is substantially smaller than the driving force, independently on how it is partitioned into E_{r1} and E_{r2}.

It should be noted that the simulation performed above are based on a nonadiabatic model of the ET reaction, while, according to the literature, the electronic coupling for the HMB/TCNE complex is very large, of the order of 0.5 eV.[39,69] Therefore, a quantitative discrepancy between the experimentally observed and the theoretically predicted spectral effect should not be too surprising. Despite this, the change of the sign of the spectral effect upon decreasing the driving force is the same as that predicted by the simulations.

V. CONCLUSIONS

The simulations presented here and based on the nonadiabatic description of the electron transfer reaction indicate that, when ultrafast, the CR dynamics of excited donor-acceptor complex should depend on the carrier frequency of the excitation pulse. Such a dependence has been experimentally observed with several complexes in polar solvents.

It should be noted that in both single- and two-mode models, a significant spectral effect is only predicted if the nonthermal transitions are dominant. In the single dimension model, this translates into the condition that $k_{\text{eff}} \sim 1/\tau_1$. In the two mode model, this condition becomes $1/\tau_1 > k_{\text{eff}} > 1/\tau_2$.

In the low exergonicity region, the models predict different signs of the spectral effect, namely, negative for single-mode model and positive for two-mode model. The positive spectral effect is also predicted for models with higher dimension. The positive spectral effect can be observed if the probability for nonthermal reaction depends significantly on the excitation frequency. On the other hand, if the reaction occurs only nonthermally, the negative spectral effect is predicted.

These simulations offer a qualitative explanation to the experimentally observed spectral effects, such as a dependence of the magnitude of the effect on the dynamics property of the solvent and on the driving force for CR. Of course, many more measurements with different systems and different solvents should be performed in order to refine these models. However it is already clear that an adiabatic description of the electron transfer is needed for a more realistic description of these ultrafast CR processes.

ACKNOWLEDGMENTS

This work was supported by the Russian foundation for basic research grants (Grant Nos. 02-03-32275 and 02-03-81008) and by the Swiss National Science Foundation through Project No. 200020-100014.

APPENDIX A: SIMULATION METHOD

The model Eqs. (2) and (3) and the initial conditions Eq. (B18) specify two aspects of the CR: (1) the diffusive transport of the nonequilibrium initial distribution to the reactive zone and (2) the reversible electronic transitions due to delta-sink terms in Eqs. (2) and (3). The reaction dynamics in this model can be effectively calculated using the Brownian simulation approach (see, e.g., Ref. 51). We have adopted this method with some modifications of the previous algorithm[51] to account for the delta-function sinks of an arbitrary power and for the reversibility of the reaction.

In the absence of reaction, the Green's function $G_0(Q_1, Q_2, t|Q_{01}, Q_{02})$ for Eqs. (2) and (3) is written as a product of the corresponding one-dimensional Gaussian functions

$$G_0(Q_1, Q_2, t|Q_{01}, Q_{02}) = \prod_i G_0(Q_i, t|Q_{0i}), \tag{A1}$$

where

$$G_0(Q_i, t|Q_{0i}) = [2\pi\langle Q_i^2\rangle[1-\Delta_i^2(t)]]^{-1/2} \times \exp\left\{-\frac{[Q_i - \tilde{Q}_i - (Q_{0i} - \tilde{Q}_i)\Delta_i(t)]^2}{2\langle Q_i^2\rangle(1-\Delta_i^2(t))}\right\},$$

$\Delta_i(t)=\exp(-t/\tau_i)$, $\tilde{Q}_i$ $(i=1,2)$ are the coordinates of minima of the corresponding free energy surfaces ($\tilde{Q}_i=0$ for the excited state, $\tilde{Q}_i=2E_{ri}$ for the ground state).

A nonreactive Brownian trajectory is then calculated as

$$Q_i^{(n+1)}=\tilde{Q}_i+(Q_i^{(n)}-\tilde{Q}_i)\Delta_i(\delta t) + \sqrt{\langle Q_i^2\rangle[1-\Delta_i^2(\delta t)]}q_i^{(n)}, \quad \text{(A2)}$$

where δt is the time increment used for the simulations, $q_i^{(n)}$ are uncorrelated Gaussian random numbers with zero mean value and unit dispersion

$$\langle q_i^{(n)}\rangle=0, \quad \langle q_i^{(n)}q_j^{(n')}\rangle=\delta_{i,j}\delta_{n,n'}. \quad \text{(A3)}$$

A reactive event may occur when the trajectory passes over the region of surface intersection. In the case of an irreversible reaction, the survival probability of a given trajectory $\vec{Q}(t)$ is calculated as[51]

$$S^{ir}(t)=\exp\left\{-\int_0^t k[\vec{Q}(t')]dt'\right\}. \quad \text{(A4)}$$

For the delta-function sink, the integral in Eq. (A4) is transformed into a sum over the crossings

$$S^{ir}(t)=\exp\left\{-\sum_k (k_0/|v_k|)\theta(t-t_k)\right\}, \quad \text{(A5)}$$

where t_k is the time of the kth crossing over the reactive zone, v_k is the velocity component perpendicular to the term crossing line $z=Q_1+Q_2$, and $\theta(t)$ is the Heaviside step function. The summation in Eq. (A5) is performed over all t_k up to t $(t_k<t)$.

Defining

$$s_k^{ir}=\exp(-k_0/|v_k|), \quad \text{(A6)}$$

we can rewrite Eq. (A5) in the form

$$S^{ir}(t)=\prod_k [1-(1-s_k^{ir})\theta(t-t_k)]. \quad \text{(A7)}$$

This algorithm can be used for the simulations of irreversible ET reactions. The reversibility of the reaction can be accounted for by introducing an additional surface-hopping process for the Brownian trajectories Eq. (A2). Actually, s_k^{ir} gives the survival probability on the same surface after a single crossing of the reactive zone, while $1-s_k^{ir}$ is the probability of surface-hopping, which is associated with the condition $\xi_k>s_k^{ir}$, where ξ_k is an additional random number, uniformly distributed between 0 and 1.

The dynamics of the electronic states populations $P_e(t)$ and $P_g(t)$ are then easily calculated by counting the numbers of trajectories N_e and N_g on the corresponding surfaces at time t

$$P_e(t)=N_e(t)/N, \quad P_g(t)=N_g(t)/N, \quad \text{(A8)}$$

N being the total number of trajectories $[N=N_e(t)+N_g(t)=\text{const}]$.

One additional comment on Eq. (A6) is needed. The Brownian motion of a particle on a free energy surface is known to be a nondifferentiable stochastic process, and therefore a definite absolute value of the velocity $|v|$ does not exist. On a practical point of view, $|v|$, being calculated using the finite differences, strongly depends on the time increment δt. From Eq. (A2), it follows that a numerical convergence of the calculated $|v|$ values with δt cannot be achieved. However, the simulations give a rather fast convergence of the averaged result, i.e., of the population dynamics. If $\delta t\leqslant 0.01\tau_2$, the results do no longer depend on the time increment. The reason of such a convergence should be due to the fact that the average number of recrossings rises with decreasing δt.

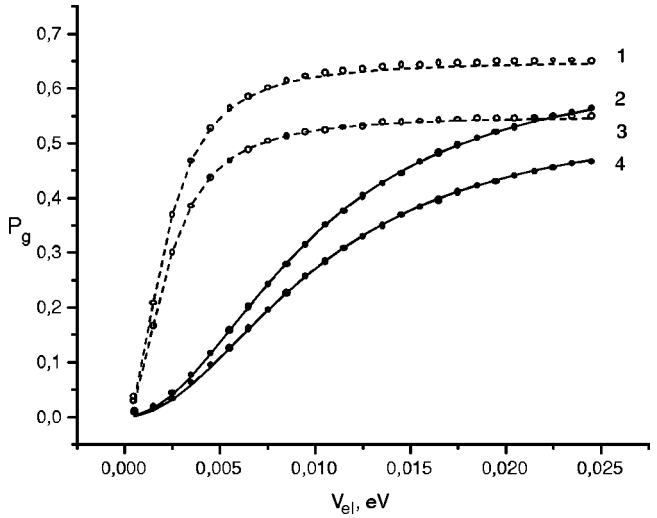

FIG. 10. Transition probabilities $P_g(t=2t^*)$ (dots) and $1-W_e$ (solid lines) [Eq. (12)] as a function of the electronic coupling V_{el}. The parameters used here are: $T=300$ K, $\tau_e=50$ fs, $E_r=1$ eV, the empty circles and the dashed lines correspond to $\tau_1=500$ fs, the filled circles and the solid lines correspond to $\tau_1=10$ ps; (1), (2) $\Delta G=-0.1$ eV; (3), (4) $\Delta G=-0.3$ eV.

The above method was first tested on simple models with known analytical solutions. A one-dimensional model[19] was used to check the program code and to find out its limits of validity. The probability of nonthermal ET $1-W_e$ has been calculated using Eq. (12).

The CR probability $P_g(t)$ in Eq. (A8) includes both the nonthermal and the thermal stages of the reaction. In order to compare $P_g(t)$ and $1-W_e$, the contribution of the thermal stage has to be removed. This condition is fulfilled by choosing $t=2t^*$, where t^* is the time at which the packet maximum passes through the point Q^*. Figure 10 shows the results of the numerical simulations of $P_g(t=2t^*)$ (dots) and $1-W_e$ [Eq. (12), solid and dashed lines] for this test model. A satisfactory agreement with the theory was achieved over its whole range of applicability including the nonadiabatic and the solvent-controlled limits, from low activation to high-barrier reactions. Most simulations were carried out with $N=10^5$. It should be noted that the stationary rates are also in good agreement with the analytical results of the one-dimensional model.[24]

It was found that there is a good accordance between the numerical data and the analytic results if the condition

$$\langle s_k\rangle\approx 1 \quad \text{(A9)}$$

is satisfied. This implies that the average probability of electronic transition upon a single crossing, $\langle p_k\rangle=1-\langle s_k\rangle$, has

to be small. This can always be fulfilled by the appropriate choice of the time increment δt. Our analysis gives the following estimation for the upper limit of δt

$$\delta t \leqslant 0.01 \min\left(\tau_L, \frac{E_r k T \hbar^2}{\pi^3 V_{\mathrm{el}}^4 \tau_L} \right). \tag{A10}$$

An analogous expression can be easily obtained for the two-dimensional model.

APPENDIX B: CALCULATION OF THE INITIAL DENSITY MATRIX

For a consistent description of the photoexcitation, the well-known analogy between the stochastic point transition model and the microscopic spin-boson model is used in this appendix to calculate the initial vibrational density matrix.[30,70] Although the result is rather simple and only reflects the overlap of the absorption and excitation pulse spectra, the calculation is described here because the result is sensitive to the short time behavior of the reaction coordinate and is only applicable if the inequality Eq. (B16) is satisfied. This restriction is inherent to the method used here to calculate the reaction dynamics.

The Hamiltonian of the spin-boson system may be written in the form[30]

$$H = \begin{pmatrix} H_e & V(t) \\ V^*(t) & H_g \end{pmatrix}, \tag{B1}$$

where

$$H_e = \frac{1}{2} \sum \ (p_\alpha^2 + \omega_\alpha^2 q_\alpha^2),$$

$$H_g = \frac{1}{2} \sum \ [p_\alpha^2 + \omega_\alpha^2 (q_\alpha - q_{\alpha 0})^2] + \Delta G$$

are the vibrational Hamiltonians of the excited and the ground electronic states

$$V(t) = -\langle e | \vec{d} \cdot \vec{E}(t) | g \rangle,$$

$\vec{d}$ is the transition dipole moment of the allowed electronic transition, $\vec{E}(t)$ is the electric pump field, and $|g\rangle$ and $|e\rangle$ are the initial ground and excited states, respectively. The optical coupling operator is expressed as

$$V(t) = V_0 \exp(-i\omega_e t - t^2/\tau_e^2),$$

where ω_e is the carrier frequency of the excitation pulse and τ_e its duration. For the sake of simplicity, we invoke the Condon approximation stating that the optical coupling operator $V(t)$ does not depend on the nuclear coordinates and momenta. ΔG is the free energy of CR, and $E_r = \Sigma A_\alpha^2 / 2\omega_\alpha^2$ is the reorganization energy, $A_\alpha = \omega_\alpha^2 q_{\alpha 0}$, q_α, p_α, ω_α and A_α being the mass-weighted coordinate, the momentum, the frequency and the electron-vibrational coupling constant for the αth mode, respectively. We use the system of units where $\hbar = 1$.

If we define the spectral density, $J(\omega)$, as

$$J(\omega) = \frac{\pi}{2} \sum \ \frac{A_\alpha^2}{\omega_\alpha} \delta(\omega - \omega_\alpha), \tag{B2}$$

then for the Debye model with

$$J(\omega) = \frac{2 E_r \omega \tau_L}{1 + \omega^2 \tau_L^2} \tag{B3}$$

the dynamics of electronic transition of the system governed by the Hamiltonian Eq. (B1) can be well fitted by Eqs. (2) and (3).[30,32]

A reaction coordinate that interacts with the electronic transition can be selected from the set of the nuclear coordinates q_α. The remaining degrees of freedom are considered as a bath. The dynamical properties of the reaction coordinate is determined by its interaction with the bath. In particular, for the Debye model of the polar solvent, one finds that the reaction coordinate motion obeys the Smoluchowski equation.[24]

The temporal evolution of the system is described by the quantum Liouville equation for the density operator ϱ

$$i \frac{\partial \varrho}{\partial t} = [H, \varrho]. \tag{B4}$$

Using the diabatic basis and the representation

$$\varrho_{ik} = e^{-iH_i t} \tilde{\varrho}_{ik} e^{iH_k t}, \quad i,j,= e,g$$

we obtain from Eq. (B4)

$$i \frac{\partial \tilde{\varrho}_{ee}}{\partial t} = V(t) T(t) \tilde{\varrho}_{ge} - \text{H.c.}, \tag{B5}$$

$$i \frac{\partial \tilde{\varrho}_{eg}}{\partial t} = V(t) T(t) \tilde{\varrho}_{gg} - V(t) \tilde{\varrho}_{ee} T(t), \tag{B6}$$

$$i \frac{\partial \tilde{\varrho}_{ge}}{\partial t} = V^*(t) T^+(t) \tilde{\varrho}_{ee} - V^*(t) \tilde{\varrho}_{gg} T^+(t), \tag{B7}$$

$$i \frac{\partial \tilde{\varrho}_{gg}}{\partial t} = V^*(t) T^+(t) \tilde{\varrho}_{eg} - \text{H.c.}, \tag{B8}$$

where

$$T(t) = e^{iH_e t} e^{-iH_g t}. \tag{B9}$$

The system is assumed to be initially at thermal equilibrium in the ground electronic state and its nuclear density operator is $\varrho_{ij}(t \to -\infty) \to 0$ with the exception of $\varrho_{gg}(t \to -\infty) \to \varrho_{gg}^{eq} = \exp(-\beta H_g)/\mathrm{Tr} \exp(-\beta H_g)$ with $\beta = 1/k_B T$.

An integral relation between the diagonal matrix elements can now be obtained from Eqs. (B5)–(B8)

$$\tilde{\varrho}_{ee}(t) = -\int_{-\infty}^{t} dt_1 \int_{-\infty}^{t_1} dt_2 \{ V(t_1) V^*(t_2) T(t_1) \times [T^+(t_2) \tilde{\varrho}_{ee}(t_2) - \tilde{\varrho}_{gg}(t_2) T^+(t_2)] + \text{H.c.} \}. \tag{B10}$$

Equation (B10) can be solved iteratively by plugging it into itself. This results in an expansion of the density operator in powers of the off-diagonal electronic matrix element $V(t)$. To first nonvanishing order, we have for $\varrho_{ee}(t)$

$$\varrho_{ee}(t)=\int_{-\infty}^{t}dt_1\int_{-\infty}^{t_1}dt_2\{V(t_1)V^*(t_2)\times T(t_1-t)\varrho_{gg}^{eq}T^+(t_2-t)]+\text{H.c.}\}. \tag{B11}$$

In coordinate representation, we obtain

$$\begin{aligned}\langle q|T(t_1-t)\varrho_{gg}^{eq}T^+(t_2-t)|q\rangle &= e^{-i\Delta G(t_1-t_2)}\prod_\alpha \sqrt{\frac{\omega_\alpha}{\pi}}\tanh\frac{\beta\omega_\alpha}{2}\exp\{i[c_\alpha(t-t_1)\\ &-c_\alpha(t-t_2)]+i[a_\alpha(t-t_1)-a_\alpha(t-t_2)]q_\alpha\}\\ &\times\exp\left\{-\frac{\omega_\alpha}{4}\tanh\frac{\beta\omega_\alpha}{2}\left(2q_\alpha+b_\alpha(t-t_1)+b_\alpha(t-t_2)\right.\right.\\ &\left.\left.-\frac{2A_\alpha}{\omega_\alpha^2}\right)^2-\frac{\omega_\alpha}{4}\coth\frac{\beta\omega_\alpha}{2}[b_\alpha(t-t_1)-b_\alpha(t-t_2)]^2\right\},\end{aligned} \tag{B12}$$

where the initial density matrix has been taken as[71]

$$\begin{aligned}\langle q|\varrho_{gg}^{eq}|q'\rangle=\prod_\alpha \sqrt{\frac{\omega_\alpha}{\pi}\tanh\frac{\beta\omega_\alpha}{2}}&\\ \times\exp\left\{-\frac{\omega_\alpha}{4}\left[\coth\frac{\beta\omega_\alpha}{2}(q_\alpha-q'_\alpha)^2\right.\right.&\\ \left.\left.+\tanh\frac{\beta\omega_\alpha}{2}(q_\alpha+q'_\alpha-2A_\alpha/\omega_\alpha^2)^2\right]\right\},&\end{aligned}$$

$\beta=1/k_BT$. The relationship

$$\begin{aligned}e^{-iH_et}e^{iH_gt}=\exp(i\Delta Gt)\exp\left[i\sum a_\alpha(t)q_\alpha\right]&\\ \times\exp\left[i\sum b_\alpha(t)p_\alpha\right]\exp\left[i\sum c_\alpha(t)\right],&\end{aligned} \tag{B13}$$

with

$$a_\alpha=-\frac{A_\alpha}{\omega_\alpha}\sin\omega_\alpha t,\quad b_\alpha=\frac{A_\alpha}{\omega_\alpha^2}(1-\cos\omega_\alpha t),$$

$$c_\alpha=\frac{A_\alpha^2}{2\omega_\alpha}\sin\omega_\alpha t\cos\omega_\alpha t$$

is also used.

The following assumptions are made: (i) the laser pulse is short enough for the inequality $\omega_\alpha\tau_e\ll 1$ to hold for all α; (ii) the high temperature limit $\beta\omega_\alpha\ll 1$ is valid; (iii) the time of interest is $t\sim\tau_e$. Consequently, the functions in Eq. (B12) can be expanded as follows: $\sin\omega_\alpha(t-t_i)\simeq\omega_\alpha(t-t_i)$, $\cos\omega_\alpha(t-t_i)\simeq 1-[\omega_\alpha(t-t_i)]^2/2$, $i=1,2$, and $\tanh\beta\omega_\alpha/2\simeq\beta\omega_\alpha/2$. Moreover, the term in Eq. (B12) with $\coth\beta\omega_\alpha/2$ disappears. The temperature dependent term in Eq. (B12) is

$$R=\frac{\beta}{2}\sum\omega_\alpha^2[q_\alpha-f_\alpha]^2,$$

where $f_\alpha=A_\alpha/\omega_\alpha^2-[b_\alpha(t-t_1)+b_\alpha(t-t_2)]/2$.

To introduce a reaction coordinate, we perform an orthogonal transformation,

$$y_i=\sum B_{i\alpha}q_\alpha,\quad \sum B_{i\alpha}B_{j\alpha}=\delta_{ij}, \tag{B14}$$

where $B_{1\alpha}=A_\alpha/\lambda$ and $\lambda^2=\Sigma A_\alpha^2$. The reaction coordinate (the collective electronic gap coordinate) is then $Q_1=\lambda y_1$. The orthogonality conditions Eq. (B14) give only $n(n+1)/2$ independent equations for the n^2 matrix elements $B_{i\alpha}$, where n is the dimensionality of the coordinate space. Having determined the coordinate y_1, one can impose more $(n-1)(n-2)/2$ conditions for $B_{i\alpha}$. The transformation becomes uniquely determined if the following additional conditions are used:

$$\sum_\alpha\omega_\alpha^2B_{i\alpha}B_{j\alpha}=\Omega_i^2\delta_{ij},\quad i,j\neq 1.$$

This leads to the expression

$$\begin{aligned}R=\frac{\beta}{2}\left\{\sum\Omega_i^2\left(y_i+\frac{D_iy_1-F_i}{\Omega_i^2}\right)^2+\Omega_1^2y_1^2\right.&\\ \left.+2\left[\sum\frac{D_iF_i}{\Omega_i^2}-\frac{1}{\lambda}\sum\omega_\alpha^2A_\alpha f_\alpha y_1\right]-\sum\frac{F_i^2}{\Omega_i^2}\right\},&\end{aligned}$$

where

$$D_i=\frac{1}{\lambda}\sum\omega_\alpha^2A_\alpha B_{i\alpha},\quad F_i=\sum\omega_\alpha^2f_\alpha B_{i\alpha},\quad \Omega_1^2=\frac{\lambda^2}{2E_r}.$$

Using the short time approximation

$$f_\alpha\simeq A_\alpha/\omega_\alpha^2-(A_\alpha/4)\varepsilon(t,t_1,t_2),$$

with $\varepsilon(t,t_1,t_2)=(t-t_1)^2+(t-t_2)^2$, and integrating over all coordinates except the reaction coordinate, the reduced density matrix is derived

$$\begin{aligned}\langle Q_1|T(t_1-t)\varrho_{gg}^{\text{eq}}T^+(t_2-t)|Q_1\rangle&\\ =Z^{-1}\exp\{-i(\Delta G-E_r-\tilde{Q}_1)(t_1-t_2)\}&\\ \times\exp\left\{-\frac{\beta}{2}\left[\frac{\tilde{Q}_1^2}{2E_r}+\frac{\lambda^2\varepsilon(t,t_1,t_2)}{4E_r}\tilde{Q}_1\right]\right\},&\end{aligned} \tag{B15}$$

where $\tilde{Q}_1=Q_1-2E_r$, Z is a normalization factor, and the following identity has been used:

$$\sum_{i,j\neq 1}\frac{B_{i\alpha}B_{i\beta}}{\Omega_i^2}A_\alpha\omega_\alpha^2A_\beta\omega_\beta^2=\sum A_\alpha^2\omega_\alpha^2-\frac{\lambda^2}{2E_r}.$$

For the Debye spectral density Eq. (B3), the integral

$$\lambda^2=\frac{2}{\pi}\int_0^\infty\omega J(\omega)d\omega$$

is divergent at the upper limit. This is a well known problem[72] and a cutoff value ω_c is used to regularize the divergence. In the limit $\omega_c\tau_L\gg 1$, we obtain $\lambda^2\simeq 2E_r\omega_c/\tau_L$. Inserting Eq. (B15) into Eq. (B11) and assuming the following inequality to be satisfied,

$$\frac{\omega_c \tau_e^2}{\tau_L} \frac{|\tilde{Q}_1|}{4k_B T} \ll 1, \tag{B16}$$

we finally find the diagonal elements of the density matrix

$$\varrho_{ee}(Q_1,0) = Z^{-1} \exp\left\{ - \frac{(Q_1 - \overline{Q}_1)^2}{2\sigma^2} \right\}, \tag{B17}$$

where $\sigma^2 = (\tau_e^2 + \tau_b^2)^{-1}$, $\tau_b^2 = 1/(2E_r k_B T)$, $\overline{Q}_1 = 2E_r + \delta\omega_e \sigma^2 \tau_e^2$, and $\delta\omega_e = \omega_e + \Delta G - E_r$.

This result can be straightforwardly generalized to a model involving several Debye-like modes

$$\varrho_{ee}(\vec{Q},0) = Z^{-1} \exp\left\{ - \frac{(\delta\omega_e - \Sigma \tilde{Q}_i)^2 \tau_e^2}{2} - \sum \frac{\tilde{Q}_i^2}{4E_{ri} k_B T} \right\}, \tag{B18}$$

where $\vec{Q} = (Q_1, Q_2, \ldots, Q_s)$, $\tilde{Q}_i = Q_i - 2E_{ri}$, and E_{ri} is the reorganization energy of the ith mode with a relaxation time τ_i. It follows from Eq. (B18) that the initial position of the wave packet maximum is

$$\overline{Q}_i = 2E_{ri}\left(1 + \frac{\delta\omega_e \tau_e^2 \sigma^2}{2E_r} \right), \tag{B19}$$

where σ is the same as in Eq. (B17) and now determines the dispersion of the initial distribution in the direction normal to the term crossing line, $E_r = \Sigma E_{ri}$. The distribution along the term crossing line is thermal. For a reorganization energy of order of 1 eV, room temperature and pulse duration of tens of femtoseconds, the inequality $\tau_e \gg \tau_b$ holds. In this case Eq. (B19) may be written as

$$\overline{Q}_i = 2E_{ri}\left(1 + \frac{\delta\omega_e}{2E_r} \right). \tag{B20}$$

The shift of the wave packet maximum upon variation of the pulse frequency can be easily seen from Eq. (B20).

[1] A. Zewail, Science **242**, 1645 (1988).
[2] M. Vos, J.-C. Lambry, S. Robles, D. Youvan, J. Breton, and J.-L. Martin, Proc. Natl. Acad. Sci. U.S.A. **88**, 8885 (1991).
[3] P. Reid, C. Silva, P. Barbara, L. Karki, and J. Hupp, J. Phys. Chem. **99**, 2609 (1995).
[4] K. Wynne, G. Reid, and R. Hochstrasser, J. Chem. Phys. **105**, 2287 (1996).
[5] N. Bakhshiev, Opt. Spectrosc. **16**, 446 (1964).
[6] V. Hizhnyakov and I. Y. Tekhver, Phys. Status Solidi **21**, 75 (1967).
[7] Y. Mazurenko and N. Bakhshiev, Opt. Spectrosc. **28**, 490 (1970).
[8] L. Zusman and A. Helman, Opt. Spectrosc. **53**, 248 (1982).
[9] B. Bagchi, D. Oxtoby, and G. Fleming, Chem. Phys. **86**, 25 (1984).
[10] G. V. der Zwan and J. Hynes, J. Phys. Chem. **89**, 4181 (1985).
[11] R. Loring, Y. Yan, and S. Mukamel, J. Chem. Phys. **87**, 5840 (1987).
[12] G. Walker, E. Akesson, A. Johnson, N. Levinger, and P. Barbara, J. Phys. Chem. **96**, 3728 (1992).
[13] M. Tachiya and S. Murata, J. Am. Chem. Soc. **116**, 2434 (1994).
[14] Y. Tanimura and S. Mukamel, J. Chem. Phys. **101**, 3049 (1994).
[15] R. Coalson, D. Evans, and A. Nitzan, J. Chem. Phys. **101**, 436 (1994).
[16] M. Cho and R. Silbey, J. Chem. Phys. **103**, 595 (1995).
[17] W. Domcke and G. Stock, Adv. Chem. Phys. **100**, 1 (1997).
[18] J. Jean, J. Phys. Chem. **102**, 7549 (1998).
[19] A. Ivanov and V. Potovoi, Chem. Phys. **247**, 245 (1999).
[20] A. Ivanov, F. Belikeev, R. Fedunov, and E. Vauthey, Chem. Phys. Lett. **372**, 73 (2003).
[21] K. Ando and H. Sumi, J. Phys. Chem. B **102**, 10991 (1998).
[22] D. Egorova, M. Thoss, W. Domcke, and H. Wang, J. Chem. Phys. **119**, 2761 (2003).
[23] K. Wynne and R. Hochstrasser, Adv. Chem. Phys. **107**, 263 (1999).
[24] L. Zusman, Chem. Phys. **49**, 295 (1980).
[25] B. Yakobson and A. Burshtein, Chem. Phys. **49**, 385 (1980).
[26] R. Marcus and N. Sutin, Biochim. Biophys. Acta **811**, 265 (1985).
[27] D. Calef and P. Wolynes, J. Phys. Chem. **87**, 3387 (1983).
[28] J. Hynes, J. Phys. Chem. **90**, 3701 (1986).
[29] E. Pollak, H. Grabert, and P. Hanggi, J. Chem. Phys. **91**, 4073 (1989).
[30] A. Garg, J. Onuchic, and V. Ambegoakar, J. Chem. Phys. **83**, 4491 (1985).
[31] M. Basilevsky and A. Voronin, J. Chem. Soc., Faraday Trans. **93**, 989 (1997).
[32] P. Frantsuzov, J. Chem. Phys. **111**, 2075 (1999).
[33] S. Ojima, H. Miyasaka, and N. Mataga, J. Phys. Chem. **94**, 7534 (1990).
[34] T. Asahi and N. Mataga, J. Phys. Chem. **95**, 1956 (1991).
[35] E. Akesson, G. Walker, and P. Barbara, J. Phys. Chem. **95**, 4188 (1991).
[36] K. Tominaga, D. Kliner, A. Johnson, N. Levinger, and P. Barbara, J. Phys. Chem. **98**, 1228 (1993).
[37] E. Lenderink, K. Duppen, and D. Wiersma, Chem. Phys. Lett. **211**, 503 (1993).
[38] S. Schneider, W. Stammler, R. Bierl, and W. Jaeger, Chem. Phys. Lett. **219**, 433 (1994).
[39] K. Wynne, C. Galli, and R. Hochstrasser, J. Chem. Phys. **100**, 4797 (1994).
[40] P.-Y. Cheng, D. Zhong, and A. Zewail, Chem. Phys. Lett. **242**, 369 (1995).
[41] H. Miyasaka, S. Kotani, and A. Itaya, J. Phys. Chem. **99**, 5757 (1995).
[42] Y. Kimura, Y. Takebayashi, and N. Hirota, Chem. Phys. Lett. **257**, 429 (1996).
[43] I. Rubtsov and K. Yoshihara, J. Phys. Chem. **101**, 6138 (1997).
[44] W. Jarzeba, S. Murata, and M. Tachiya, Chem. Phys. Lett. **301**, 347 (1999).
[45] E. Vauthey, J. Phys. Chem. **105**, 340 (2001).
[46] O. Nicolet and E. Vauthey, J. Phys. Chem. **106**, 5553 (2002).
[47] Q. Zhong, Z. Wang, Y. Sun, Q. Zhu, and F. Kong, Chem. Phys. Lett. **248**, 277 (1996).
[48] A. Ovchinnikov and M. Ovchinnikova, Zh. Eksp. Teor. Fiz. [Sov. Phys. Dokl. **29**, 688 (1969)] **56**, 1278 (1969).
[49] S. Garg and C. Smyth, J. Phys. Chem. **69**, 1294 (1965).
[50] B. Bagchi and N. Gayathri, Adv. Chem. Phys. **107**, 1 (1999).
[51] D. Bicout and A. Szabo, J. Chem. Phys. **109**, 2325 (1997).
[52] L. Zusman, Chem. Phys. **119**, 51 (1988).
[53] N. Mataga, T. Asahi, Y. Kanda, T. Okada, and T. Kakitani, Chem. Phys. **127**, 249 (1988).
[54] M. Horng, J. Gardecki, A. Parazyan, and M. Maroncelli, J. Phys. Chem. **99**, 17311 (1995).
[55] T. Joo, Y. Jia, J.-Y. Yu, M. Lang, and G. Fleming, J. Chem. Phys. **104**, 6089 (1996).
[56] J. Gumy, O. Nicolet, and E. Vauthey, J. Phys. Chem. **103**, 10737 (1999).
[57] A. Barzykin, P. Frantsuzov, K. Seki, and M. Tachiya, Adv. Chem. Phys. **123**, 511 (2002).
[58] A. Shushin, Chem. Phys. Lett. **60**, 149 (1981).
[59] P. Frantsuzov and M. Tachiya, J. Chem. Phys. **112**, 4216 (2000).
[60] O. Nicolet, A. Ivanov, and E. Vauthey, in *Femtochemistry and Femtobiology: Ultrafast Events in Molecular Science*, edited by J. T. Hynes and M. Martin, (Elsevier, Amsterdam 2004) p. 331.
[61] M. Mobley, K. Rieckhoff, and E.-M. Voigt, J. Phys. Chem. **81**, 809 (1977).
[62] E.-M. Voigt, J. Am. Chem. Soc. **86**, 3611 (1999).
[63] C. Hoegemann, M. Pauchard, and E. Vauthey, Rev. Sci. Instrum. **67**, 3449 (1996).
[64] T. Shida, *Electronic Absorption Spectra of Radical Ions; Physical Sciences Data*, Vol. 34 (Elsevier, Amsterdam, 1988).
[65] S. Pagès, B. Lang, and E. Vauthey, J. Phys. Chem. **108**, 549 (2004).
[66] O. Edholm and C. Blomberg, Chem. Phys. **252**, 221 (1999).
[67] F. Markel, N. Ferris, I. Gould, and A. Myers, J. Am. Chem. Soc. **114**, 6208 (1992).
[68] I. Gould and S. Farid, J. Phys. Chem. **96**, 7635 (1992).
[69] C. Jurgensen, M. Peanasky, and H. Drickamer, J. Chem. Phys. **83**, 6108 (1985).
[70] I. Rips and J. Jortner, J. Chem. Phys. **87**, 2090 (1987).
[71] R. Feynman, *Statistical Mechanics* (Benjamin, New York, 1972).
[72] W. Unruh and W. Zurek, Phys. Rev. D **40**, 1071 (1989).